Investigation of turbulence in reversed field pinch plasma by using microwave imaging reflectometry

Z. B. Shi, Y. Nagayama, S. Yamaguchi, Y. Hamada, Y. Hirano, S. Kiyama, H. Koguchi, C. A. Michael, H. Sakakita, and K. Yambe

Citation: Physics of Plasmas (1994-present) **18**, 102315 (2011); doi: 10.1063/1.3652848
View online: http://dx.doi.org/10.1063/1.3652848
View Table of Contents: http://scitation.aip.org/content/aip/journal/pop/18/10?ver=pdfcov
Published by the AIP Publishing

Investigation of turbulence in reversed field pinch plasma by using microwave imaging reflectometry

Z. B. Shi,[1,2] Y. Nagayama,[3] S. Yamaguchi,[4] Y. Hamada,[3] Y. Hirano,[5] S. Kiyama,[5] H. Koguchi,[5] C. A. Michael,[6] H. Sakakita,[5] and K. Yambe[7]
[1]*The Graduate University for Advanced Studies, Toki 509-5292, Japan*
[2]*Southwestern Institute of Physics, Chengdu 610041, China*
[3]*National Institute for Fusion Science, Toki 509-5292, Japan*
[4]*Kansai University, Suita 564-8680, Japan*
[5]*Advanced Industrial Science and Technology, Tsukuba 305-8568, Japan*
[6]*UKAEA, Abingdon, Oxfordshire OX14 3DB, United Kingdom*
[7]*Osaka University, Osaka 565-0871, Japan*

(Received 16 June 2011; accepted 26 September 2011; published online 21 October 2011)

Turbulence in the reversed field pinch (RFP) plasma has been investigated by using the microwave imaging reflectometry in the toroidal pinch experiment RX (TPE-RX). In conventional RFP plasma, the fluctuations are dominated by the intermittent blob-like structures. These structures are accompanied with the generation of magnetic field, the strong turbulence, and high nonlinear coupling among the high and low k modes. The pulsed poloidal current drive operation, which improves the plasma confinement significantly, suppresses the dynamo, the turbulence, and the blob-like structures. © *2011 American Institute of Physics*. [doi:10.1063/1.3652848]

The reversed field pinch (RFP) is a toroidal plasma confinement system with a unique feature that the toroidal field is reversed at the edge.[1] The RFP configuration is sustained by a dynamo action. As the dynamo is also a mechanism of generation and sustainment of the magnetic field in the universe,[2] the dynamo is an important issue in the plasma physics. It is considered that the dynamo is driven by the turbulence so that the plasma confinement in conventional RFP is poor.[2] The tearing instabilities are dominant in RFP.[1] So the current drive can stabilize the magnetic fluctuation and improve the confinement. The pulsed poloidal current drive (PPCD) has been demonstrated in MST and used in other RFP devices.[3,4] In PPCD plasma, the external electric field is generated by the current in the coil embedded in the toroidal field coil.[5] This external electric field can drive the poloidal current so that the reversal field can be sustained without the help of the electromotive force driven by fluctuation. Therefore, PPCD sustains the reversed field externally and improves the confinement significantly.[3,6] Turbulence must play an important role in this case. Despite its importance, measurements of the turbulence have been limited at the edge plasma region in RFP so far.[7,8]

This paper presents the first fluctuation measurement near the reversal surface by using the microwave imaging reflectometry (MIR).[9–13] In a conventional reflectometer, the reflected signal contains components from multiple fragmented wave fronts caused by turbulence, resulting in a complicated interference pattern at the detector plane, and the assumption of the simple relation between the signal and the density fluctuation fails. In an MIR system, a wide aperture optical system is used to form an image of the reflected surface onto the detector array located at the image plane. As a result, MIR signal is the reflection of microwave from the fluctuation of the reflection surface, which corresponds to the equi-density surface. Significant observation is as follows: the shape of reflection surface in conventional RFP is a blob-like structure and that in PPCD plasma is sinusoidal. This may be the reason why PPCD improves the plasma confinement significantly.

Figure 1 shows the schematic diagram of the MIR system in the toroidal pinch experiment RX (TPE-RX), which is a large RFP device with the major radius of $R = 1.72$ m and the minor radius of $a = 0.45$ m (Ref. 14). Details of the MIR system have been reported previously.[12,13] In this system, the plasma is illuminated by the O-mode microwave with the frequency of 20 GHz, which corresponds to the cutoff density of $\sim 0.5 \times 10^{19}$ m^{-3}. The image of the cutoff surface is made onto the imaging detector by the optical system (M_1, M_2). The imaging detector is made of a 4×4 planar Yagi-Uda antenna array on a teflon printed circuit board. The spatial resolution is 3.7 cm in toroidal and poloidal directions. The reflected microwave signal can be written as $Ae^{i\phi}e^{i\omega t}$, where ω is the microwave frequency, A and ϕ are the amplitude and the phase, respectively. In the simulation and the laboratory test, we found that the phase ϕ corresponds to the displacement of the cutoff surface in the radial direction and the amplitude A corresponds to the shape of the cutoff surface.[15] The amplitude A and phase ϕ are detected by an RF detector and a quadrature detector, respectively. The quadrature detector provides the in-phase ($I \sim \cos\phi$) and quadrature ($Q \sim \sin\phi$) signals.

Figure 2 shows the plasma current (I_p), the reversal parameter ($F = B_t(a)/\langle B_t \rangle$), the central chord soft X-ray (SXR), the central chord line averaged density ($n_{ea}(\times 10^{19}$ m$^{-3})$), the normalized cutoff radius (r_{cut}), the amplitude signals of MIR and their wavelet spectra in typical examples of the PPCD and the conventional RFP plasmas. The plasma density is measured by a dual-chord interferometer in TPE-RX. One chord views the center and the other one views at r/a = 0.69. The density profile is estimated by fitting the experimental data with $n(r,t) = ne(0,t)(1 - r^4)(1 + Cr^4)$, where C is the profile factor. $C > 0$ denotes the hollow density profile, and $C < 0$ denotes the peaked density profile.[13] The

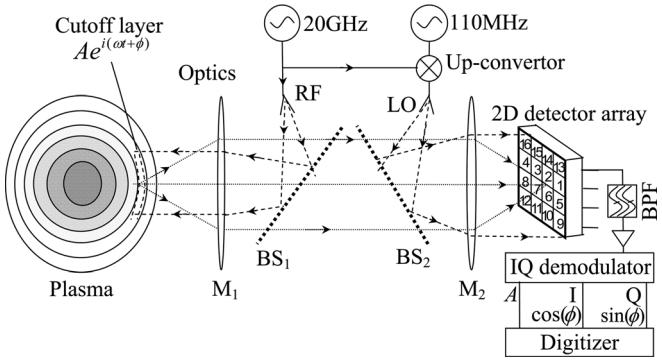

FIG. 1. Schematic diagram of the MIR system in TPE-RX.

normalized cutoff radius ($r_{cut}=a_{cut}/a$) can be obtained, where a_{cut} is the real cutoff radius and a is the plasma minor radius. The electron density profile is usually flat or hollow in TPE-RX. Both the PPCD and the conventional RFP plasmas have similar cutoff surface ($r_{cut}\approx 0.8$) during the flattop of the plasma current. The PPCD operation starts at $t=18$ ms when F is rapidly decreased. We may use F as a parameter of the self generated reversed field, but this usage of F is valid only in conventional RFP plasmas. The deeper F corresponds to the stronger dynamo in conventional RFP plasmas, but dynamo may be absent in PPCD plasmas. Interestingly, the fluctuation level in MIR signal is similar, while the SXR intensity of the PPCD plasma is 100 times higher than that in the conventional RFP plasma. Since the density

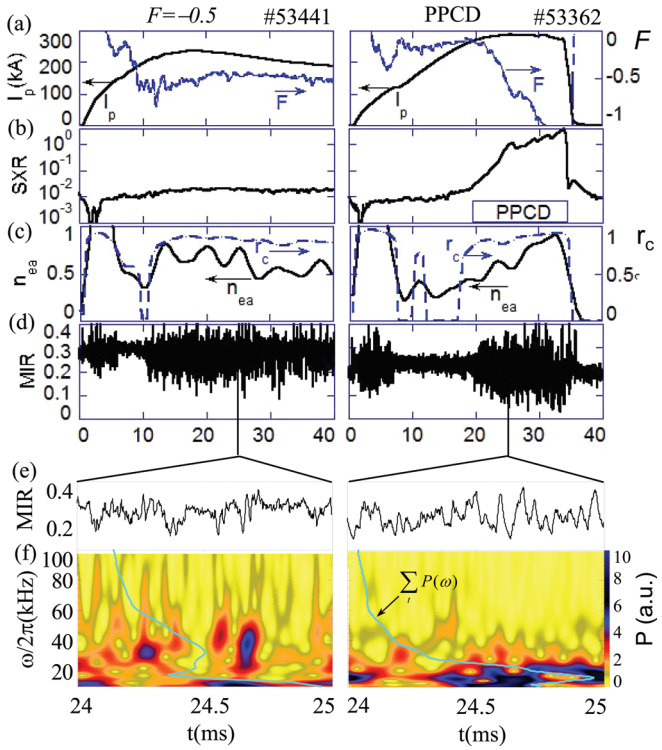

FIG. 2. (Color) Plasma parameters and MIR signals in the conventional RFP (left) and the PPCD (right) plasmas in TPE-RX. (a) The plasma current (I_p) and reversal parameter (F), (b) the central chord soft X-ray (SXR), (c) the central chord line averaged density ($n_{ea}(\times 10^{19}$ m^{-3})), (d) normalized cutoff radius (r_{cut}), (e) the amplitude signal of MIR (ch.2), and (f) wavelet spectrum. The line in Fig. 2(f) denotes the sum of wavelet spectrum. $\sum P(\omega)$.

is similar, this high SXR intensity indicates that the PPCD operation improves the plasma stored energy significantly.

Since the turbulence is composed of many short lived waves, the wavelet analysis is a powerful tool to analyze the turbulence.[16,17] The wavelet transform of the signal $x(t)$ is defined as

$$P(s,\tau)=\frac{1}{\sqrt{s}}\int x(t)\Psi^*(s,t-\tau)dt \qquad (1)$$

where the superscript * denotes the complex conjugate, s is the time scale ($s=2\pi/\omega$), and

$$\Psi(s,t)=\frac{1}{\pi^{1/4}}\exp\left[-i\left(\frac{2\pi t}{s}\right)-\frac{1}{2}\left(\frac{t}{s}\right)^2\right] \qquad (2)$$

is the Morlet function. Figure 2(f) shows the wavelet spectra of the MIR signals. The summed power spectra $\sum P(\omega)$ are also shown. In the conventional RFP plasma, the spectrum has many short lived structures among intermittent bursts with broad frequency spectra. In the PPCD plasma, the high frequency fluctuation is suppressed and the spectrum is dominated by the frequency of ~20 kHz.

Figure 3 shows the 2D wavenumber (k) spectra in the conventional RFP and PPCD plasmas. Here, k_φ and k_θ are the toroidal and the poloidal wavenumbers, respectively. These spectra are obtained by using the 2D maximum entropy method (MEM).[18,19] In the PPCD plasma, the fluctuation power is localized in the low k_θ and low k_φ range as $k_\theta=0\pm 20$ m^{-1}, $k_\varphi=0\pm 10$ m^{-1}. The spectrum of the conventional RFP plasma distributes in a wide k range, as $k_\theta=-20\sim 20$ m^{-1} and $k_\varphi=-40\sim 20$ m^{-1}. Since the observed plasma region ($r_{cut}\approx 0.8$) is near the reversal surface, the magnetic field is mainly poloidal as indicated by an arrow in Fig. 3. Therefore, the spectrum spreads in the electron drift direction which is perpendicular to the magnetic field. This broad k spectrum is consistent with the idea that the conventional RFP plasma is in the multi-helicity state. The magnetic fluctuation in the conventional RFP plasma is much stronger than that in the PPCD plasma. The mode analysis of the magnetic signals indicates that the $m=0$ tearing mode is dominant in the conventional RFP plasma. In the

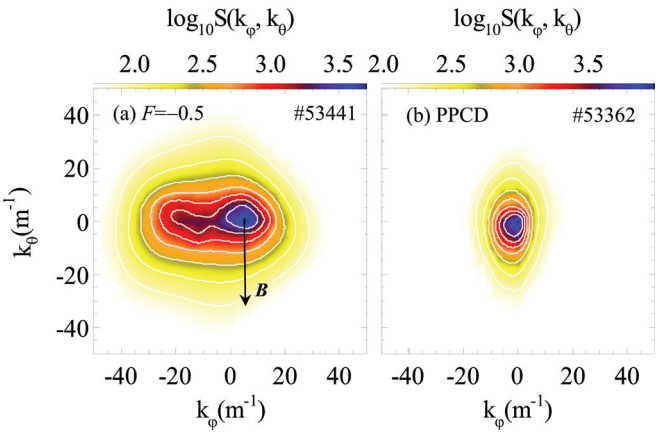

FIG. 3. (Color) The 2D spectra ($\log_{10} S(k_\phi, k\theta)$) of (a) the conventional RFP and (b) the PPCD plasmas estimated by MEM.

PPCD plasma, the edge dynamo is suppressed and the $m=1$ mode is dominant.[6]

Assume a toroidal periodic condition on the fluctuation, the time evolution of the k spectrum on the cutoff surface can be obtained by the spatial Fourier transform of MIR signals

$$S(k,t)=\sum_{l=0}^{L-1} x(l,t)e^{i2\pi kl/L}, \tag{3}$$

where L is the total toroidal detector number. Here, the complex MIR signal, $x(l,t)$, is defined as $x(l,t)=A(I+iQ)$. The complex signal represents the amplitude and phase of the density fluctuation simultaneously.[15] By taking the spatial Fourier transform of the data obtained by four detectors along the toroidal direction, we obtain the components of wavenumbers of $k=-0.5k_N$, 0, $0.5k_N$, k_N, where $k_N=84\ \mathrm{m}^{-1}$ is the Nyquist wavenumber, which corresponds to the wavelength of 7.4 cm. They correspond to the toroidal mode numbers of $n=-73$, 0, 73, 146, respectively. The minus indicates the opposite propagation direction. Hereafter, we use the normalized wavenumber ($k_a \equiv 2k/k_N$), as $k_a=-1$, 0, 1, 2 for convenience.

Now, let us write (k_1, k_2, k_3) for the nonlinear interaction among the three waves of k_1, k_2, and k_3. The squared wavelet bicoherence (b^2) is useful to quantify the strength of the nonlinear three wave interaction.[16] This is defined as

$$b^2=\frac{|\langle P_{k_1}(s_1,\tau)P_{k_2}(s_2,\tau)P^*_{k_3}(s_3,\tau)\rangle|^2}{\langle|P_{k_1}(s_1,\tau)P_{k_2}(s_2,\tau)|^2\rangle\langle|P_{k_3}(s_3,\tau)|^2\rangle}, \tag{4}$$

where $\langle\rangle$ is the ensemble average over time and τ. $P_k(s,\tau)$, is the Morlet wavelet transform of the waves defined as Eq. (1). Within the frequency resolution, the time scale should satisfy the frequency sum rule: $1/s_3=1/s_1+1/s_2$, which is equivalent to $\omega_3=\omega_1+\omega_2$, as $\omega/2\pi=1/s$.

The bicoherence is higher than the noise level in the case of the matched coupling condition, $k_1+k_2=k_3$. The matched couplings of (−1,1,0) and (1,1,2) represent the nonlinear interactions among different turbulent scales. Figure 4 shows typical squared wavelet bicoherence spectra of (−1,1,0). The wavelet transform is performed within 8 ms during the flattop of the plasma current. The coupling is strong in the high frequency range (50 ~ 200 kHz) in the conventional RFP plasma ($F=-0.5$), as shown in Fig. 4(a).

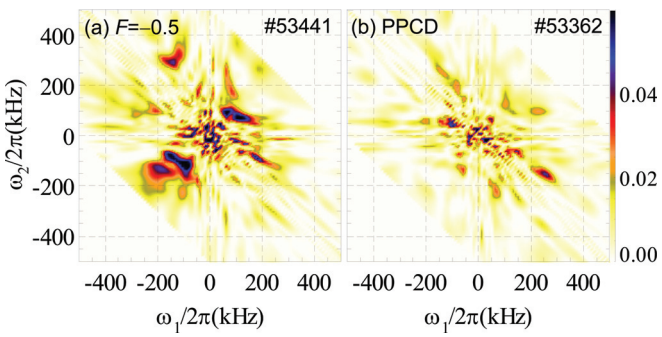

FIG. 4. (Color) Squared wavelet bicoherence spectra of (−1,1,0) in (a) conventional RFP ($F=-0.5$) and (b) PPCD plasmas.

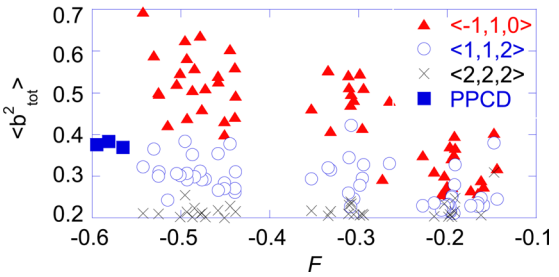

FIG. 5. (Color online) Total wavelet bicoherence of (−1,1,0), (1,1,2), and (2,2,2) as a function of F.

The strength of the nonlinear interaction may be compared by using the total bicoherence, $b^2_{tot}=\sum b^2(s)$, where the sum is taken over all time scales s. Figure 5 shows the total bicoherence as a function of F. Generally, the bicoherence of the mismatched coupling condition, $k_1+k_2\neq k_3$, should be as small as the noise level.[16] The matched couplings such as (−1,1,0) is distinctly stronger than the mismatched one (2,2,2) in the conventional RFP plasma, as shown in Figs. 4(a) and 5. The low k coupling (−1,1,0) is stronger than the high k coupling (1,1,2). In conventional RFP plasmas, the total bicoherence of (−1,1,0) is increased as F becomes deeper ($-F$ is increased). This suggests that the nonlinear coupling of turbulence is related to the dynamo. In the PPCD plasma, the matched coupling of (−1,1,0) is much smaller than that in the deep F ($F<-0.3$) plasma, as shown in Figs. 4(b) and 5. This may be due to the absence of the dynamo. Note, the measured $k_a=0$ mode contains all low k modes ($|k|<21\ \mathrm{m}^{-1}$), and the $k_a=1$ corresponds to the high k turbulence ($21\ \mathrm{m}^{-1}<k<63\ \mathrm{m}^{-1}$).

Generally, a turbulence signal has an intermittent nature. Figures 6(b)–6(f) show the time evolutions of magnetic

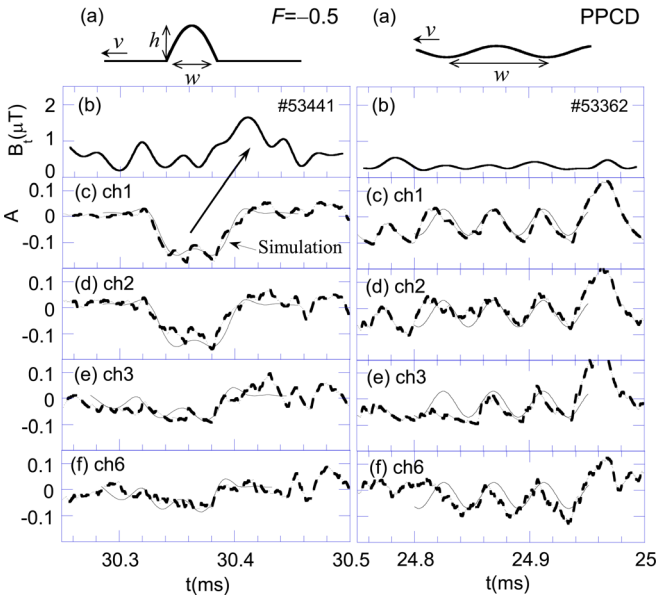

FIG. 6. (Color online) (a) Blob-like shape of the cutoff surface (w = 5 cm, $h=1$ cm) in the conventional RFP plasma (left) and sinusoidal shape of the cutoff surface (w = 157 cm, $h=0.375$ cm) in the PPCD plasma (right). Time evolutions of (b) the magnetic fluctuation and (c)-(f) the MIR signals. Thin solid line indicates simulated signal with the model (a). Thick broken line indicates the experimental signal.

signal and MIR signals, respectively. In the conventional RFP plasma, the fluctuations have the features of intermittency, which is enhanced as the F becomes deeper. This corresponds to the negative spikes in the MIR signal, as shown in Fig. 2(e). A strong negative burst is observed in ch.1 and ch.2 at $t = 30.33$ ms. Here, MIR channel numbers are shown in Fig. 1. Right after this burst, a positive burst is observed in the magnetic signal. This burst is a typical intermittent phenomenon.

As MIR signal is a microwave reflection, the shape of the cutoff surface can be estimated from the measured signal. A model based on the Huygens-Fresnel equation is developed to simulate the propagation of the reflected signal in the optical system.[15] It is found that the optical system can make a clear image of the cutoff surface as $4k_{\perp}hL/D < 1$, where D is the diameter of the optical lens, L is the distance between the optical lens and the cutoff surface, $k_{\perp}$ is the perpendicular wavenumber, and h is the height of the fluctuation. In general, high $k_{\perp}$ fluctuations have small radial displacement in the experiment. The measured $k_{\perp}h$ is determined by the geometrical parameter of the optical system. The fluctuations in TPE-RX mainly distribute in the range of $4k_{\perp}hL/D < 0.8$, which suggests that the present MIR optical system can make a clear image of the cutoff surface in plasma.

Figure 6(a) shows the estimated reflection surface that is characterized by the width (w) and the height (h). Here, the width ($w = 2\pi/k_{\perp}$) is estimated from the two-point cross correlation method and the height (h) is estimated from the phase fluctuation. In the case of conventional RFP plasma, the negative spike of MIR signal can be simulated by a single interchange (blob-like) structure characterized by ($w = 5$ cm, $h = 1$ cm). This blob-like structure modulates the cutoff surface, scatters the reflection wave, and leads to the rapid decrease of the reflection power. This structure appears at $t = 30.37$ ms, and the magnetic field is increased at $t = 30.42$ ms. This process corresponds to the nonlinear evolution from the intermittency to the generation of the magnetic field. In the case of PPCD plasma, the fluctuation of MIR signal is not intermittent but is an oscillating wave with the frequency of ~20 kHz, which is compatible with the magnetic fluctuation, as shown in Fig. 6 (right side). The reflection surface in the PPCD plasma can be estimated as a sinusoidal shape with ($w = 157$ cm, $h = 0.375$ cm), which corresponds to the toroidal mode $n = 7$.

In the case of conventional RFP plasma, the present observation is summarized as follows: the fluctuation has broad k spectrum in the electron drift direction; high k modes in the opposite directions and a low k mode are strongly coupled; fluctuation of the equi-density surface has a blob-like structure; the magnetic field is increased in a short period right after the blob-like structure generation. In the case of PPCD plasma, the present observation is summarized as follows: the MIR signal has narrow k spectrum; fluctuation of the equi-density surface has a sinusoidal shape; the soft X-ray intensity is 100 times higher than the conventional RFP plasma.

In the magnetohydrodynamic (MHD) dynamo model,[2] the parallel mean-field Ohm's law can be written as

$$\eta j_{\parallel} = E_{\parallel} + \langle \tilde{v} \times \tilde{B} \rangle_{\parallel}, \tag{5}$$

where $\langle\rangle$ indicates the average over an equilibrium flux surface, $\parallel$ denotes parallel to the magnetic field, $E_{\parallel}$ is the parallel external electric field, $j_{\parallel}$ is the parallel equilibrium current, and η is the parallel electric resistivity. The fluctuating fluid velocity and magnetic field, $\tilde{v}$ and $\tilde{B}$, can be caused by the turbulence. In the conventional RFP plasma, the mode coupling of high k modes probably generates the blob-like interchange mode, which makes large $\tilde{v}$ in the radial direction. So, the dynamo term, $\langle \tilde{v} \times \tilde{B} \rangle_{\parallel}$, drives the poloidal current that generates the toroidal field. In the case of PPCD operation, the second term of Eq. (5) is diminished as $\tilde{v} = 0$. Probably, the external field, $E_{\parallel}$, which is provided by PPCD, replaces the dynamo term in Eq. (5).

In conclusion, the blob-like interchange activity is observed by using MIR in the conventional RFP plasma. This activity may cause both the energy loss and the dynamo. The poloidal current drive near the reversal surface suppresses this activity and improves the plasma confinement.

This work is supported by the NINS Imaging Science Project (Grant No. NIFS08KEIN0021), SOKENDAI (Grant No. NIFS08GLPP003), and the Budget for Nuclear Research of the Ministry of Education, Culture, Sports, Science and Technology of Japan.

[1]H. A. B. Bodion, Nucl. Fusion, **30**, 1717 (1990).
[2]H. Ji and S. C. Prager, Magnetohydrodynamics **18**, 191 (2002).
[3]J. S. Sarff, S. A. Hokin, H. Ji, S. C. Prager, and C. R. Sovinec, Phys. Rev. Lett. **72**, 3670 (1994).
[4]Y. Yagi, Y. Maejima, H. Sakakita, Y. Hirano, H. Koguchi, T. Shimada, and S. Sekine, Plasma Phys. Controlled Fusion **44**, 335 (2002).
[5]H. Koguchi, H. Sakakita, S. Kiyama, K. Yambe, T. Asai, Y. Hirano, F. Auriemma, D. Terranova, and P. Innocente, Plasma Fusion Res. **4**, 022 (2009).
[6]L. Frassinetti, Y. Yagi, H. Koguchi, T. Shimada, and Y. Hirano, Phys. Plasmas **11**, 5229 (2004).
[7]S. Assadi, S. C. Prager, and K. L. Sidikman, Phys. Rev. Lett. **69**, 281 (1992).
[8]R. Cavazzana, G. Serianni, P. Scarin, M. Agostini, N. Vianello, Y. Yagi, H. Koguchi, S. Kiyama, H. Sakakita, and Y. Hirano, Plasma Phys. Controlled Fusion **49**, 129 (2007).
[9]E. Mazzucato, Nucl. Fusion **41**, 203 (2001).
[10]E. Mazzucato, T. Munsat, H. Park, B. H. Deng, C. W. Domier, N. C. Luhmann, A. J. H. Donn, and M. J. van de Pol, Phys. Plasmas **9**, 1955 (2002).
[11]H. Park, C. C. Chang, B. H. Deng, C. W. Domier, A. J. H. Donn, K. Kawahata, C. Liang, X. P. Liang, H. J. Lu, N. C. Luhmann, A. Mase, H. Matsuura, E. Mazzucato, A. Miura, K. Mizuno, T. Munsat, Y. Nagayama, M. J. van de Pol, J. Wang, Z. G. Xia, and W-K. Zhang, Rev. Sci. Instrum. **74**, 4239 (2003).
[12]S. Yamaguchi, Y. Nagayama, R. Pavlichenko, S. Inagaki, Y. Kogi, and A. Mase, Rev. Sci. Instrum. **77**, 10E930 (2006).
[13]Y. Nagayama, S. Yamaguchi, Z. B. Shi, Y. Kogi, A. Mase, S. Sugito, Y. Hirano, S. Kiyama, H. Koguchi, H. Sakakita, K. Yambe, and N. Ohyabu, Plasma Fusion Res. **3**, 053 (2008).
[14]Y. Yagi, S. Sekine, H. Sakakita, H. Koguchi, K. Hayase, Y. Hirano, I. Hirota, S. Kiyama, Y. Maejima, Y. Sato, T. Shimada, and K. Sugisaki, Fusion Eng. Des. **45**, 409 (1999).
[15]Z. B. Shi, Y. Nagayama, D. Kuwahara, T. Yoshinaga, M. Sugito, and S. Yamaguchi, J. Plasma Fusion Res. **8**, 109 (2009).
[16]B. P. van Milligen, C. Hidalgo, and E. Snchez, Phys. Rev. Lett. **74**, 395 (1995).
[17]Z. B. Shi, Y. Nagayama, S. Yamaguchi, Y. Hamada, and Y. Hirano, Plasma Fusion Res. **3**, S1045 (2008).
[18]J. Skilling and R. K. Bryan, Mon. Not. R. Astron. Soc. **211**, 111 (1984).
[19]Z. B. Shi, Y. Nagayama, S. Yamaguchi, D. Kuwahara, T. Yoshinaga, M. Sugito, Y. Hirano, H. Koguchi, S. Kiyama, H. Sakakita, K. Yambe, and C. Michael, Plasma Fusion Res. **5**, S1019 (2010).